Analyst

Accepted Manuscript

ROYAL SOCIETY OF CHEMISTRY

www.rsc.org/analyst

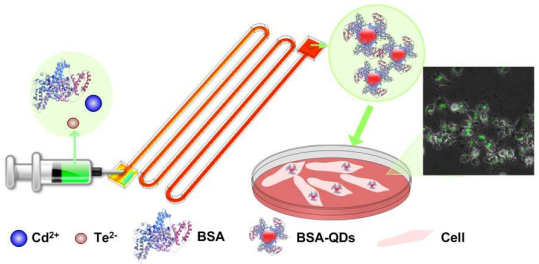

Biofunctionalized quantum dots were prepared using microfluidic chips and they were used as optical probes for imaging of live cells.

Preparation of Biofunctionalized Quantum Dots Using Microfluidic Chips for Bioimaging

Siyi Hu[1,2,4#], Shuwen Zeng[2,3#], Butian Zhang[2], Chengbin Yang[2], Peiyi Song[2], Tng Jian Hang Danny[2], Guimiao Lin[5], Yucheng Wang[2], Tommy Anderson[2], Philippe Coquet[3], Liwei Liu[1,4]*, Xihe Zhang[1,4] and Ken-Tye Yong[2]*

[1]School of Science, Changchun University of Science and Technology, Changchun 130022, Jilin, China

Email: liulw@cust.edu.cn

[2]School of Electrical and Electronic Engineering, Nanyang Technological University, Singapore 639798, Singapore

E-mail: ktyong@ntu.edu.sg

[3]CINTRA CNRS/NTU/THALES, UMI 3288, Research Techno Plaza, 50 Nanyang Drive, Border X Block, Singapore 637553, Singapore

[4]International Joint Research Center for Nanophotonics and Biophotonics, Changchun University of Science and Technology, Changchun 130022, Jilin, China

[5]The Engineering Lab of Synthetic Biology and the Key Lab of Biomedical Engineering, School of Medicine, Shenzhen University, Shenzhen 518060, China

[#]These authors contributed equally to this work

Abstract

Biofunctionalized quantum dots (QDs), especially protein-coated QDs, are known as useful targeted fluorescent labels for cellular and deep-tissue imaging. These nanoparticles can also serve as efficient energy donors in fluorescence resonance energy transfer (FRET) binding assays for multiplexed sensing of tumor markers. However, current preparation processes for protein-functionalized QDs are laborious and require multiple synthesis steps (e.g. preparing them in high temperature, making them dispersible in water, and functionalizing them with surface ligands) to obtain high quality and quantity of QD formulations. This significantly impedes the progress of employing QDs for clinical diagnostics use such as QDs-based immunohistofluorescence assay. Here, we demonstrate a one-step synthesis approach for preparing protein-functionalized QDs by using microfluidic (MF) chip setup. Using bovine serum albumin (BSA) molecules as the surface ligand model, we first studied and optimized the MF reaction synthesis parameters (e.g. reaction temperature, channel width and length)

for making protein-functionalized QDs using COMSOL simulation modeling followed by experimental verification. Moreover, in comparison with the BSA-functionalized QDs synthesized from conventional bench-top method, BSA-QDs prepared using MF approach exhibit a much higher protein-functionalization efficiency, photostability and colloidal stability. The proposed one-step MF synthesis approach will provide a rapid, cost effective, and small-scale production of nanocrystals platform for developing new QD formulations in applications ranging from cell labeling to sensing of biomolecules. Most importantly, this approach will greatly reduce the chemical waste produced during the trial-and-error stage of developing and perfecting the desired physical and optical property of new QDs materials.

1. Introduction

Microfluidic chips are promising platform for lab-on-a-chip applications such as single cell analysis, chemical sensing, and contaminants monitoring in water[1-6]. With flow channel dimension in a scale of hundreds of micrometers, small amounts of sample fluids (nanoliter to picoliter volume) can be processed or manipulated within the MF chip [7]. Upon comparing to conventional hot colloidal synthesis method, using microfluidic chip to prepare desired QDs displays several unique advantages: (i) small quantity of materials and reagents are needed for making the QDs and this will avoid generating large volume of chemical wastes; (ii) microfluidic chip allows one to fabricate QDs within minutes and this will allow one to rapidly test a series of QDs recipes by employing multiple MF chips for the reaction to take place; (iii) the reaction temperature, reagent mixing and reaction time for QDs synthesis can be precisely controlled and this will generate a much narrower particle-size distribution [8]; (iv) low thermal mass and large surface to volume ratio of the MF channels allow rapid heat transfer to the desired reaction region which will help to promote homogeneous nucleation of QD seeds and this will produce QDs fluorescence spectrum with desired emission peaks [8]; (v) the microfluidic devices can be modified and integrated with additional parts for preparing multifunctional and multimodal QDs for in vivo imaging [9, 10] and drug delivery therapy applications [11, 12]. The first nanoparticle synthesis using microfluidic chip was reported by Mello's group in 2002 [13]. They demonstrated that the polydispersity of CdS nanoparticles was significantly reduced by using a continuous flow-based microfluidic chip setup. Since then, various metallic, metal oxide, magnetic and semiconductor nanoparticles such as Ag [14, 15], Au [16, 17], Co [18, 19], TiO_2 [20-22], Fe_3O_4 [23], SiO_2 [24], CdSe [25-27], CdTe [8], ZnSe [28], PbS [8], InP [29] and even more complicated core/shell nanostructures such as CdSe/ZnS [30], Fe_2O_3/SiO_2 [31], ZnSe/ZnS [32], ZnS/CdSe/ZnS [33] have been successfully prepared using microfluidic devices [34]. It is worth

noting that the reproducibility of making nanoparticles with identical physical and chemical property can be achieved by using microfluidic chip and this will be beneficial in producing high quality QDs-based assays (e.g. immunofluorescence assay) for clinical diagnosis applications [35].

Among the above-mentioned nanoparticles, colloidal QDs have attracted great attention from biomedical and life science research communities due to their usefulness for bioimaging and drug screening applications [36-38]. For instance, the emission peak of CdTe QDs can be tuned from visible to near-infrared (NIR) wavelength region by changing their particle size [39] and such unique feature will allow one to use them for multicolor fluorescence imaging of cells [40]. Carbon nanodots (CQDs) and graphene quantum dots (GQDs) are another class of promising nanoparticles for bioimaging and nanomedicine use. We foresee that such nanoparticles are more acceptable for clinical studies since they are made from benign carbon material [41-45]. To apply QDs for imaging and sensing applications such as optical immunosensing and in vivo tumor imaging, the QDs needs to be functionalized with targeting ligands (e.g. protein, DNA, RNA, peptides and lipids) for targeted labeling of desired cells and biomarkers [46]. To date, direct synthesis of biofunctionalized QDs still remains as a challenge yet to be overcome. Very little success has been achieved by using the conventional bench-top synthesis method to produce biofunctionalized QDs in a single step. This is mainly due to the following reasons: (i) high temperature (higher than 100 ℃) and long-hours reaction time (more than 10 hours) are required to produce high crystalline QDs and such harsh environment process will generally degrade the biomolecules; (ii) if the synthesis process of QDs is carried out under a mild condition, the photoluminescence intensity, optical and colloidal stability of biofunctionalized QDs will be significantly compromised. Currently, the preparations of biofunctionalized QDs require complex and tedious steps such as solubilization of QDs in water, functionalization of biomolecules, and purification of QDs to accomplish [47, 48]. Thus, there is a need to engineer new approaches to rapidly synthesize biofunctionalized QDs in a single step method thereby allowing one to use these QDs for biological use without the need of any other processing steps.

In this work, we report the use of microfluidic chip for one-step synthesis of BSA-functionalized CdTe QDs and this approach address the main challenges faced by conventional synthesis method. Prior fabricating microfluidic chip for QDs synthesis, we first employed COMSOL Multiphysics finite element simulation technique to design and optimize

the microfluidic reaction channel parameters (e.g., reaction temperature, channel width and length) for preparing QDs in a Laminar Flow model. Once our device design was optimized, these parameters were used as references to fabricate microfluidic chip for making QDs in aqueous phase. The prepared BSA-QDs from the microfluidic chip device (MF) were then characterized by UV-Vis absorbance (Abs) and photoluminescence (PL) spectroscopy, Fourier transform infrared spectroscopy (FT-IR) and agarose gel electrophoresis. Upon comparing to the BSA-QDs that were obtained from conventional bench-top colloidal synthesis method (BT), BSA-QDs synthesized by microfluidic device displayed higher degree of functionalization of BSA and significant improvement in the optical and colloidal stability of QDs. In addition, we even demonstrated that this MF method can be extended to prepare QDs functionalized with folic acids and these bioconjugates can be used for targeted imaging of cancer cells.

2. Results and discussion

In our one-step synthesis of CdTe QDs using MF approach, 3-Mercaptopropionic acid (MPA) and BSA molecules are used as surface ligands to stabilize and control the growth of the QDs in aqueous dispersion. Basically, BSA molecules will bind to the QDs surface through coordination of amino acid residues with Cd^{2+} ions, while MPA molecules will passivate the QDs surface for enhancing the colloidal stability of the nanocrystals. In this work, we first investigate the effects of reaction temperature on the growth rate of QDs in the microfluidic chip. By using the Reaction Engineering (*re*) model in COMSOL Multiphysics 4.3a, the relationship between the concentration of the synthesized QD and the residence time (i.e., the reaction time of QDs inside the microfluidic channel) can be theoretically predicted. The initial concentrations of Cd^{2+} and Te^{2-} solutions injected into the inlets of microfluidic chip is set to be 10 mM and 3.3 mM and this provides a Cd/Te concentration ratio of 1:0.3. This ratio is fixed in all of our experimental and simulation works. When the reaction temperature increases from 50 to 100 ℃, the concentration of QDs increases from 1.6 mM to 2.4 mM after 5 mins reaction time (see Figure 1a) and this indicates elevating the reaction temperature will promote a faster growth rate of QDs. The distribution profiles of concentrations of BSA-QDs synthesized in the microfluidic reaction channel of 200 μm height and 200 μm width at various reaction temperatures (50, 65, 85 and 100 ℃) are plotted in Figure 2. We then carried out the actual synthesis of QDs with MF approach under the same reaction temperatures for verification with the simulation data. In Figure 1b, one can clearly see that the total particles number of synthesized BSA-QDs increases as the reaction temperature increases. The

number of generated QDs increases from 1.90×10^{18} L^{-1} to 3.19×10^{18} L^{-1} when temperature increases from 50 to 100 ℃. The obtained experimental result agrees well with the simulation data. In our case, the QD particles number was estimated by using Beer–Lambert law [49] and we assumed the size of the CdTe to be 1.5 nm in the estimation since the emission peaks of the prepared QD products are mostly centered at 460 nm. To further understand the effects of reaction temperatures on the growth kinetics of QDs, one-step MF synthesis of MPA-attached CdTe QDs is also demonstrated. In this experiment, BSA molecules are not utilized because the reaction temperatures used here are greater than 100^{o}C and this will denature the protein molecules. Thus, we have used MPA molecules instead that can withstand higher reaction temperature. Simulation result in Figure 3a showed that the concentration of MPA-CdTe QD products increased from 2.4 mM to 4.5 mM after 5 mins of reaction time with the reaction temperature increasing from 98 to 220 ℃. Similarly, a same trend is observed in the experimental result where we have prepared CdTe QDs at reaction temperatures ranging from 98 to 220 ℃, as shown in Figure 3b. The total particles number of MPA-CdTe QDs is estimated to increase from 3.18×10^{18} to 4.37×10^{18} L^{-1} when higher temperature is applied during the synthesis process. For directly preparing QDs aqueous dispersion in three-neck flask, the maximum reaction temperature that can be applied is around 100 ℃ and further increment of temperature will result in vaporizing the reaction medium and disrupting the colloidal and optical stability of the QDs [40, 50]. Such challenges can be easily overcome by using MF synthesis method. As the reaction mixture is enclosed in a small space, the MF reaction temperature for aqueous phase QDs synthesis can be raised above 100 ℃ without the need of worrying the evaporation of the reaction solution during the fabrication process. Actually, we demonstrate that MPA-CdTe QDs can be synthesized at temperature as high as 200^{o}C and in general this will produce high crystalline QDs with better quantum yield. More importantly, this will significantly reduce the reaction time for producing per batch QDs since rapid heat transfer can be achieved in short burst by the high surface to volume ratio (SA:V) (~5000 m^{-1}) of the reaction channels (see equation 1) and the low thermal mass of the reagents travelling within the channel system [51].

$$\frac{WL}{WLH} = \frac{1}{H} \tag{1}$$

In equation 1, W refers to the width of the channel, L is the channel length and H is the channel height. Based on the fact and above-mentioned results, one can prepare multiple batches of QDs with different functionalities within 30 minutes by using the MF method and

this will significantly improve the procedures in optimizing the intended QDs formulations for specific biological applications.

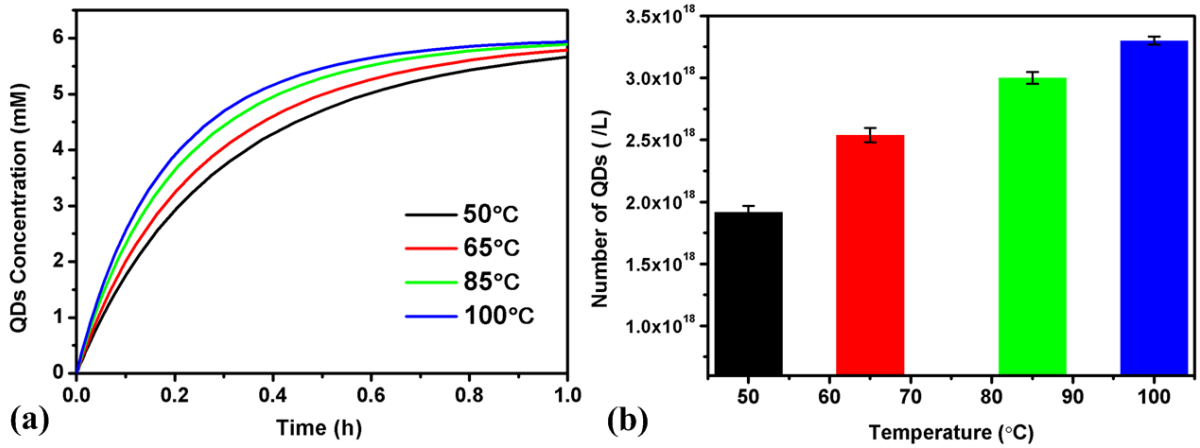

Figure 1 Simulation results (a) and experimental measurements (b) of BSA-QDs synthesized via MF method under different reaction temperatures (50, 65, 85 and 100 ℃). All the experiments in Fig. 1b were carried out with the same reaction time of 5 min.

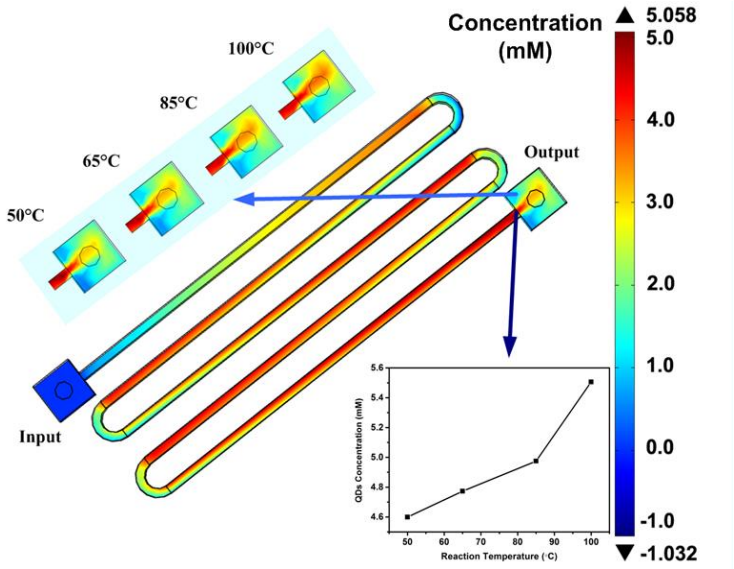

Figure 2 Simulation prediction of the concentration distribution of BSA-QDs synthesized in the microfluidic channel with a width of 200 μm under different reaction temperatures (50, 65, 85 and 100 ℃).

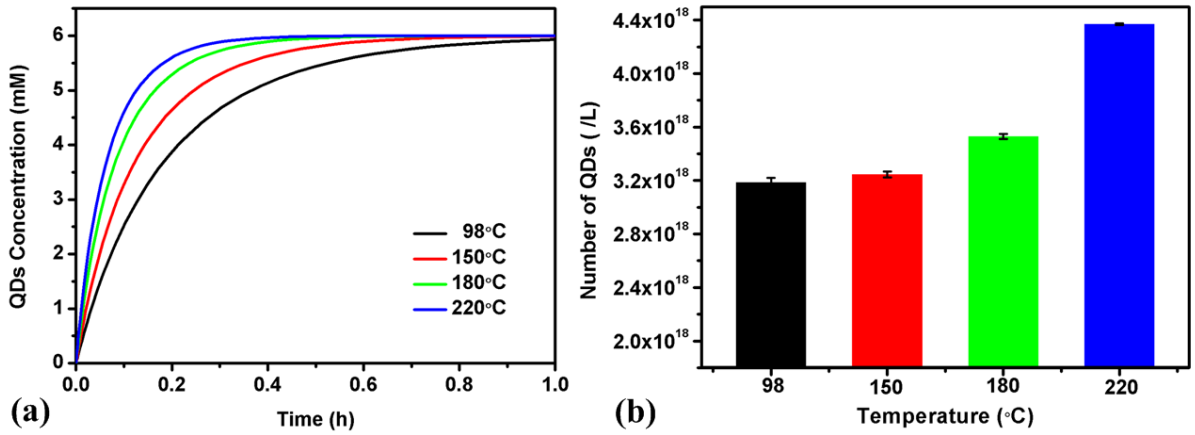

Figure 3 Simulation results (a) and experimental measurements (b) of MPA-CdTe QDs in aqueous phase synthesized via MF method under different reaction temperatures (98, 150, 180 and 220 ℃). All the experiments in Figure 3b were carried out with the same reaction time of 5 mins.

In order to confirm the attachment of BSA molecules on the QDs surface, agarose gel electrophoreses experiments are performed for the as-prepared QDs sample. From Figure 4, one can see that the MPA-coated CdTe QDs exhibited a single band (upper band) with high mobility while BSA-conjugated QDs exhibited another band (lower band) with retarded mobility due to their relatively large size when compare to that of MPA-QDs. We have observed that the luminescence intensity of BSA-QDs synthesized at 65 ℃ (lower band) is much stronger than that of the ones synthesized at 85 and 100 ℃. Moreover, no luminescence intensity is observed from the upper band of BSA-QDs prepared at 65 ℃, indicating that most of QDs are passivated with BSA molecules. The obtained gel electrophoresis result suggested that BSA molecules were mostly denatured under high reaction temperatures at 85 and 100 ℃. In addition to agarose gel electrophoreses, surface compositions of BSA-QDs synthesized at 65 ℃ have been characterized by FTIR spectrometer (see Figure 5). The broad peaks of free BSA at 3448 cm^{-1}, BSA-Cd^{2+} ion at 3442 cm^{-1} and MF-BSA-QD at 3445 cm^{-1} are attributed to the O-H stretch of the BSA phenol group [52]. The blue shift of this broad peak from 3448 cm^{-1} indicated that the BSA phenol group of tyrosine residue had interacted with Cd^{2+} and CdTe QDs. The peaks of free BSA at 1653 cm^{-1} and 1454 cm^{-1} are respectively due to the C=O stretch of the carboxyl group from glutamine and C-N stretch of the imidazole group from histidine residue. The intensities of these two peaks were significantly attenuated in the spectra of BSA-Cd^{2+} ion and MF-BSA-QD complex, indicating the respective reaction of the carboxyl group and histidine residue with Cd^{2+} and CdTe QDs. The new peak of BSA-Cd^{2+} at 1107 cm^{-1} might be contributed to the interaction between Cd^{2+} and BSA. The peaks of BSA-(MPA) Cd^{2+} and MF BSA-(MPA) CdTe at 1402 cm^{-1} were attributed to the COO^{-} of

MPA, which corresponded to the reaction of MPA with Cd^{2+} and CdTe QDs. The FTIR result suggested that the BSA molecules had initially chelated with Cd^{2+} ions and remained bound to the surface of CdTe QDs [53, 54] throughout the microfluidic synthesis process. Based on the studies elaborated above, we have chosen 65 ℃ as the optimum reaction temperature in preparing BSA-functionalized QDs using microfluidic chip for biological applications.

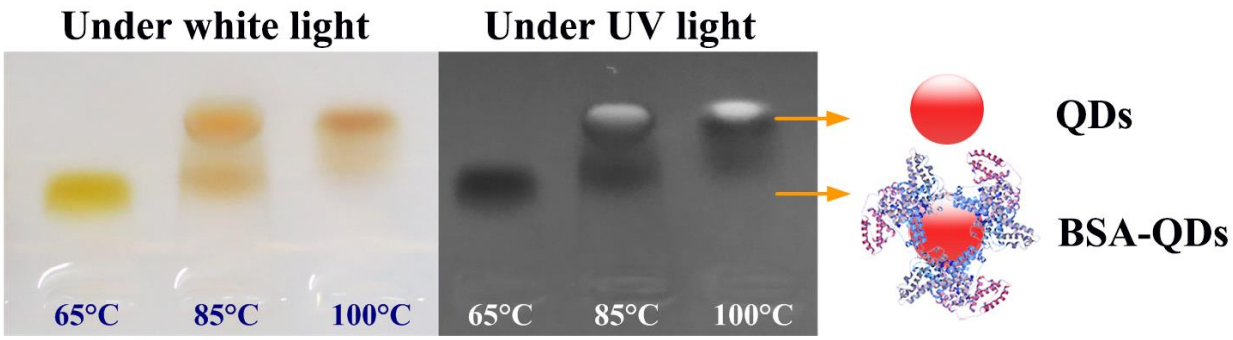

Figure 4 Agarose gel electrophoresis of BSA-QDs synthesized via MF method in 5 mins under different reaction temperatures (65, 85 and 100 ℃).

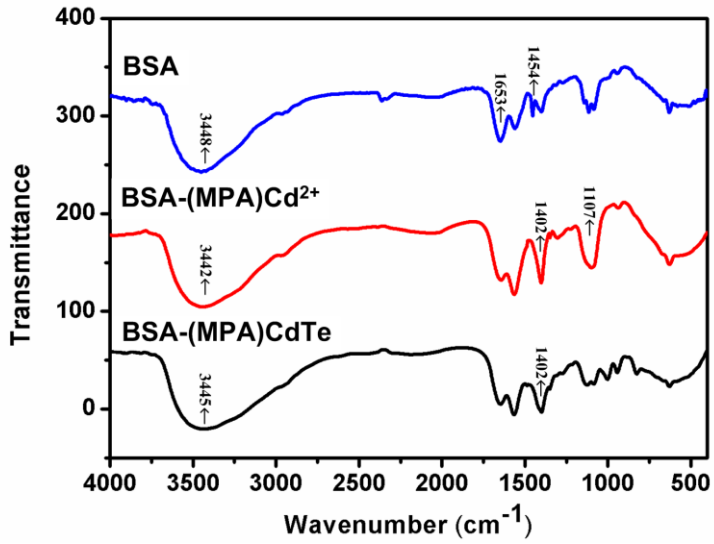

Figure 5 FTIR spectra of free BSA, BSA-Cd^{2+} ion complex and MF-BSA-QD synthesized under 65 ℃.

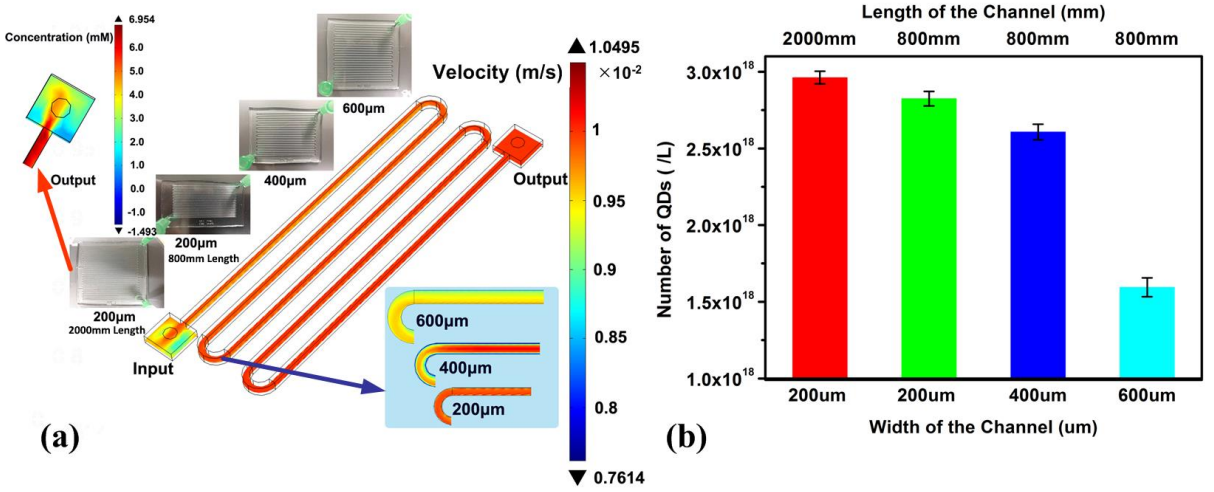

Figure 6 Simulation results (a) and experimental measurements (b) of BSA-QDs synthesized via MF method with different channel widths (200 μm, 400 μm and 600 μm) or lengths (800 mm and 2000 mm) under the optimum reaction temperature of 65 ℃. All the experiments in Figure 6b were carried out with the same reaction time of 5 mins and a fixed volumetric flow rate of 500 μL/min.

Besides from the reaction temperature, the parameters (e.g., width and length) of microfluidic channels are playing an important role in determining the final shape and size of the prepared nanoparticles as well [1, 7]. Here, we first employed the Transport of Diluted Species (*chds*) and Laminar Flow (*spf*) models in COMSOL Multiphysics 4.3a to provide a theoretical prediction on the generated QDs concentration and their corresponding velocity profiles within the MF channels. The channel height and the volumetric flow rate (i.e., the pumping rate of the syringe containing reagents) in all of the theoretical and experimental studies are fixed at 200 μm and 500 μL/min. The first parameter we investigate is the channel width of the MF system. Figure 6a shows the predicted velocity profiles of the generated QDs in the MF channels with channel widths of 200 μm, 400 μm and 600 μm, respectively. In order to save the computation time and storage space, the channel length is fixed at 50mm. The flow velocity of QDs concentration is estimated to reach the maximum state when MF with a channel width of 200 μm is used. This can be explained by Eq. (2) from which the flow velocity inside the MF channel is inversely proportional to the channel width when the channel height and volumetric flow rate are fixed [51].

$$v = \frac{Q}{A} = \frac{Q}{WH} \tag{2}$$

Here, v is the flow velocity, Q is the volumetric flow rate, A is the cross-sectional area of the microfluidic channel, W is the width of the channel and H is the channel height. To confirm and test the accuracy level of our calculation, we then carried out one-step syntheses of BSA-QDs formulation using microfluidic chips with channel widths of 200 μm, 400 μm and

600 μm and a fixed channel length of 800 mm. The reactions were carried out at the optimum reaction temperature of 65 ℃. As shown in Figure 6b, the BSA-QD particles number increases with decreasing channel width from 600 μm to 200 μm and the number of BSA-QDs particles has increased from 1.59×10^{18} L^{-1} to 2.82×10^{18} L^{-1}. This result is attributed to the higher flow velocity inside the MF channel with 200 μm that effectively prevents the deposition of QD byproducts on the channel wall. Also, the narrower MF channel width will generally lead to a more homogeneous reaction to take place and thus producing BSA-QDs particles with higher monodispersity sizes[25, 34]. The second MF parameter we investigate is the MF channel length. Simulation result in the top left inset of Figure 6a indicates that the concentration of BSA-QD particles increases from 5.058 mM to 6.954 mM when a channel length with 2.5 times longer is used. Experimental result in Figure 6b also show that BSA-QD particles number increases when the total channel length is changed from 800 mm to 2000 mm. Based on such result, we conclude that the longer MF channel length will generally generate a delay in the continuous residence time for QDs reaction (i.e., the reaction time of QDs inside the microfluidic channel) and thus creating a larger population of QDs within the channel [27, 34]. The generated BSA-QDs particles number using 2000 mm length channel is estimated to be 2.96×10^{18} L^{-1} and this value is much higher than that of the particles number produced in 800 mm length channel. From Figure 7, one can see that the PL intensity of the prepared BSA-QDs with MF channel width and length of 200 μm and 2000 mm is even much stronger than that of BSA-QDs synthesized using conventional bench-top flask method for 4 hours and this indicates that a higher growth kinetic rate of BSA-QDs can be achieved by using MF approach. The functionalization efficiency of BSA-QDs produced by MF and BT approaches are also investigated by performing agarose gel electrophoresis testing. Figure 8 shows agarose gel electrophoresis data for BSA-QDs produced using either MF or BT method. Using the same BSA concentration of 0.5 mg/mL in the MF and BT synthesis processes, the luminescence intensity from the lower band of BSA-QDs produced by MF method is much stronger than that of BSA-QDs generated using BT synthesis method. On the other hand, the luminescence intensity from the upper band of QDs prepared with MF technique is much weaker than that of QDs created with BT approach. The lane of BSA concentration of 2.0 mg/mL shows there is no QDs in the upper band and the BSA-QDs are all located at the lower band, suggesting QDs are all conjugated with BSA at the BSA concentration of 2.0 mg/mL. This comparison study clearly demonstrates that a higher functionalization efficiency of BSA molecules on the QDs surface is achieved for MF method when we compare it with BT technique, and the optimum concentration of BSA to

conjugate with QDs is 2.0 mg/mL.

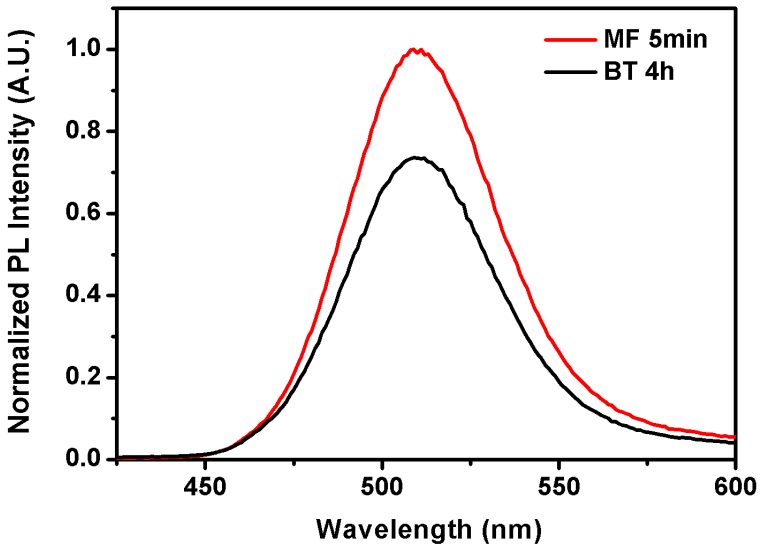

Figure 7 Photoluminescence spectra of MF-BSA-QDs synthesized in 5 mins (red line), BT-BSA-QDs synthesized in 4 hour (black line).

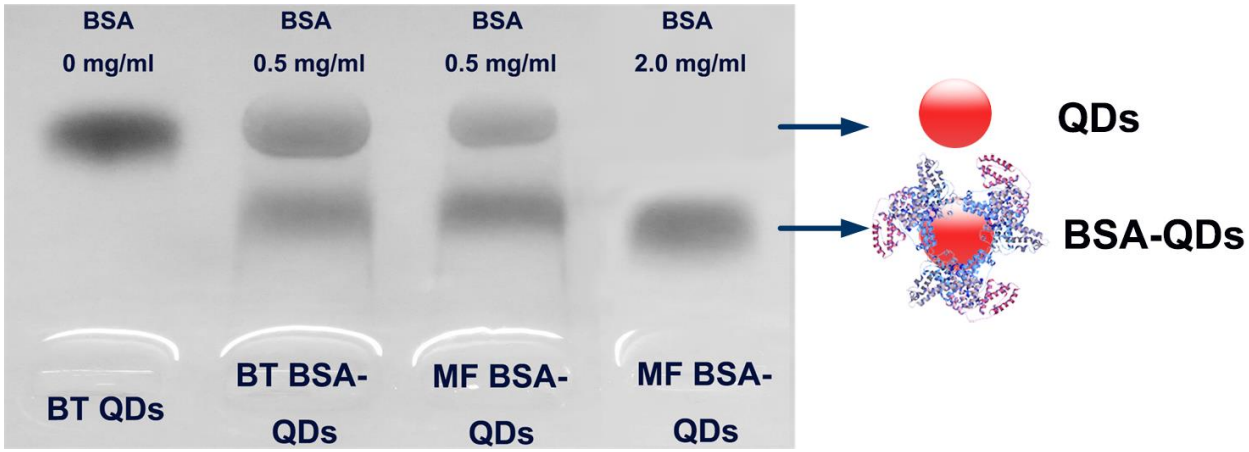

Figure 8 Agarose gel electrophoresis of BT-MPA-QDs, BT-BSA-QDs and MF-BSA-QDs synthesized in 5 mins under 65 ℃.

Photostability and colloidal stability of QDs are important factors to be considered when one is utilizing them as optical probes for biological applications such as bioimaging [55]. Figure 9 shows the PL maximum changes of BSA-QDs produced by MF and BT methods and these samples are exposed with continuous UV radiation at different time periods. The PL signals of QDs were carefully monitored and measured (Fig. S1). In our experiment, a lower photobleaching rate was observed for BSA-QDs formulation prepared by using MF method when we increased the exposure time of UV radiation to the samples. More specifically, the PL intensity drops by 74% after 7 hours of UV radiation exposure for the case of QDs produced by MF approach. But, a drop of 90% is observed for the case of QDs generated by BT method. This clearly shows that MF method produced QDs with better photostability

upon comparing to BT technique. Besides from photostability experiments, we have also performed QDs colloidal stability study. The colloidal stability of the prepared BSA-QDs is evaluated at pH values ranging from 5 to 12 for 60 hours of examination. Their hydrodynamic sizes are monitored using dynamic light scattering (DLS) technique at room temperature, as shown in Figure 10 and S2. The BSA-QDs prepared by MF and BT methods are relatively stable at pH value of 12. This may be due to the rich hydroxide ions available at high pH value that facilitated the dissociation of unbound anionic groups (e.g. carboxyl groups) on BSA ligands and thus increased the surface charge density of the QDs [56]. The BSA-QDs formulation synthesized using MF approach is much more stable in pH 5, 7 and 9 solutions when compare to those generated by BT method. It is worth noting that BSA-QDs prepared by BT method were more easily to be aggregated and precipitated out from the water when compared to those generated by MF approach. Overall, the colloidal stability of BSA-QDs generally depends on the pH value in the solution. Nevertheless, our result indicates that MF method is producing BSA-QDs formulation with much better colloidal stability.

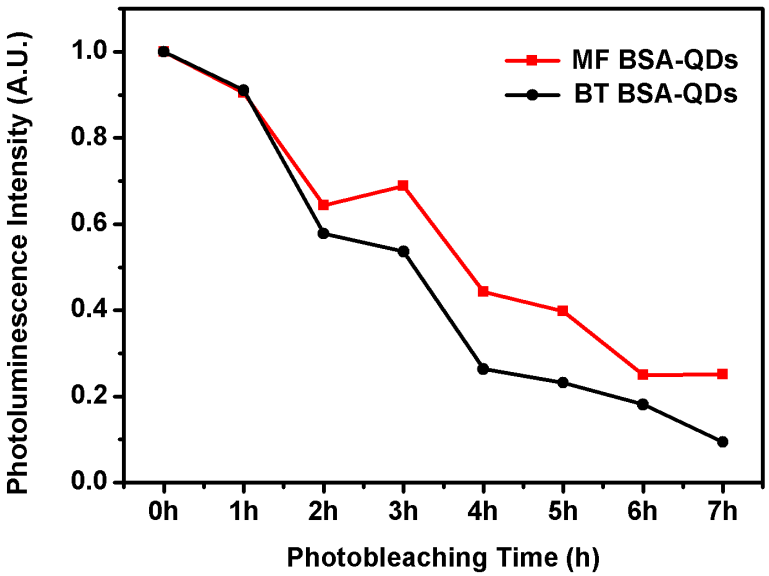

Figure 9 Comparison of photostability between MF-BSA-QDs synthesized in 5 mins and BT-BSA-QDs synthesized in 4 hours. The PL maximum changes of QDs under different UV irradiation time.

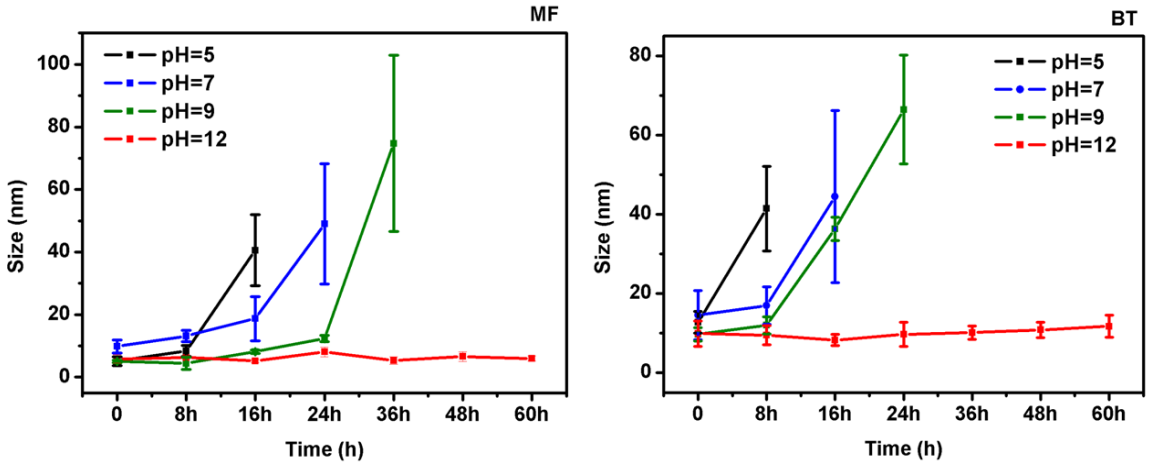

Figure 10 Comparison of colloidal stability between MF-BSA-QDs synthesized in 5 mins and BT-BSA-QDs synthesized in 4 hours at different pH values (5, 7, 9 and 12) for 60 hours.

For bioimaging study, we have employed the prepared BSA-QDs for labeling of live cells. RAW264.7 macrophages cell were used in this experiment. As illustrated in Figure 11a, a strong cellular uptake was observed for our MF-BSA-QDs formulation with a quantum yield (QY) of 16.23%. The green emission signals are originated from the prepared QDs. The result here indicates that BSA-QDs prepared by MF approach are suitable to be used as an optical contrast agent for imaging of cells and live animals. Using the same synthesis method, folic acids (FA)-functionalized CdTe QDs are also prepared in this study. FA is a commonly used cancer-homing agent for targeted drug delivery application as its corresponding receptors (folate receptors) are known to be overexpressed in a variety of cancer cells. Figure 11c shows fluorescence images of Panc-1 cells stained with FA-QD bioconjugates. From the fluorescence images, the FA-mediated targeting can be observed by the luminescent signal from the labeled cells and the QDs were located in the vesicles within the cells. On the other hand, a weak QD signal was detected from the cancer cells treated with MPA-QDs in Figure 11b, thus indicating that the QD bioconjugates uptake happened through specific interaction rather than passive uptake mechanism. In the near future, we envision that one can prepare peptide- or antibody conjugated QDs formulation using MF method and can be conveniently used for in vivo imaging of tumor vasculatures and tumor matrix.

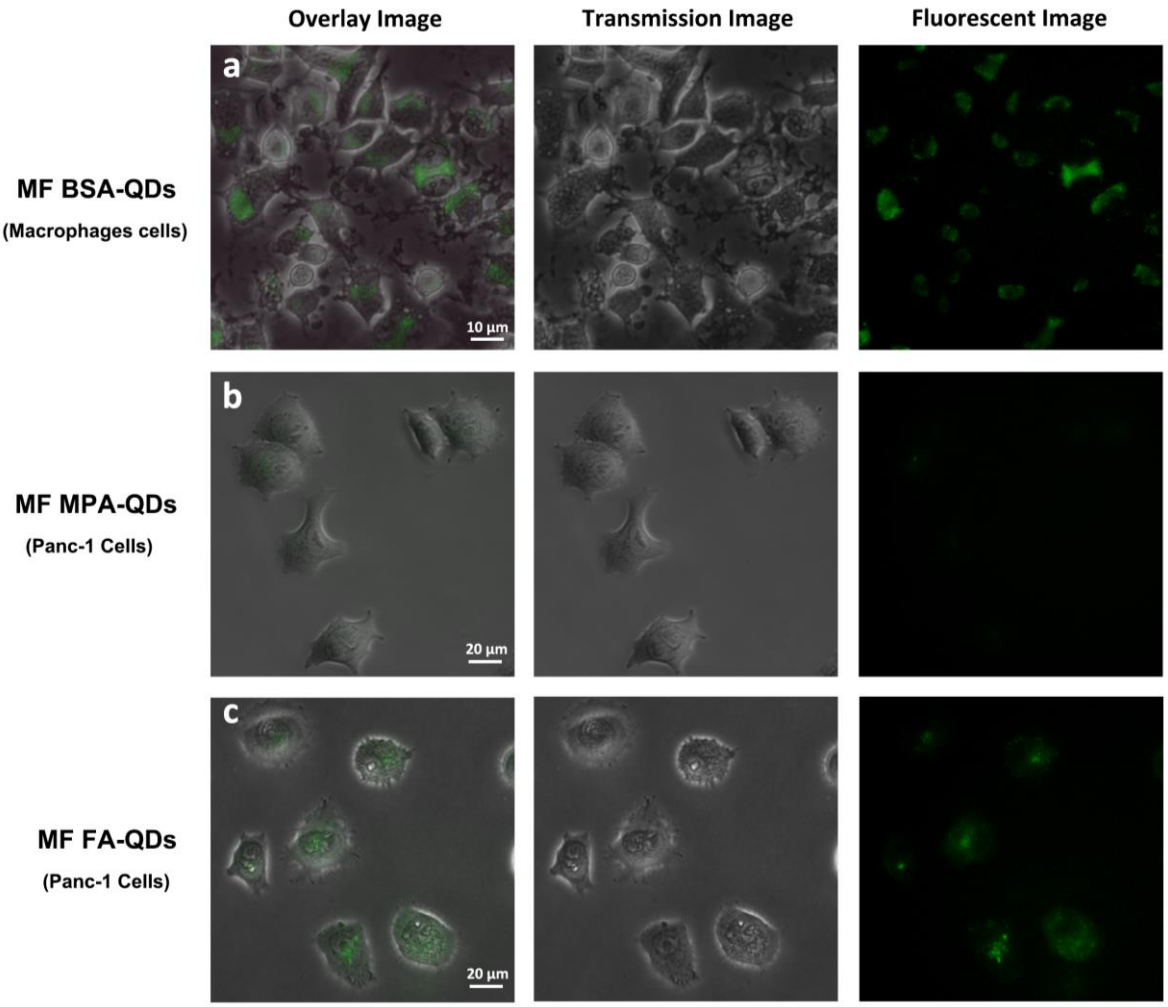

Figure 11 Microscopic images of (a) RAW264.7 cells labeled with MF-BSA-QDs, (b) Panc-1 cells labeled with MF-MPA-QDs and (c) Panc-1 cells labeled with MF-FA-QDs.

3. Conclusions

In summary, we presented a detailed study on using microfluidic chips for synthesis of BSA-conjugated CdTe QDs. We demonstrate that microfluidic chip is more convenient, time-saving and effective in preparing biofunctionalized QDs at mild temperature upon comparing to the conventional bench-top hot colloidal synthesis method. A systematic theoretical modeling was performed to investigate the impact of reaction temperature, channel width, and length of the microfluidic device on the kinetic growth rate of QDs. Thereafter, this simulated result is compared with the experimental work for further verification. Our experimental result shows good agreement with the simulation data. Both experimental and simulation works show that reaction temperature, channel width, and length of the microfluidic device play an important role in determining the flow velocity profile of the reaction agents and the final yield of QDs. Since biofunctionalized QDs can be used as

optical probes for bioimaging, our work will certainly open up an avenue for developing highly integrated microfluidic system that is capable of preparing biocompatible functionalized QDs for direct usage of cell and tumor imaging without the need of going through multiple rounds of washing, size selection and purifying of QDs particles.

4. Methods

4.1 Materials

Cadmium perchlorate hydrate (99.999%), tellurium powder (99.8%), sodium borohydride (99.99%), 3-Mercaptopropionic acid (MPA, ≥99%), albumin from bovine serum (BSA, ≥98%) and folic acid (FA, ≥97%) were purchased from Sigma-Aldrich. 10×Tris-Acetate-EDTA (TAE, pH=8.0) and agarose powder were purchased from Vivantis Ltd. Sodium hydroxide (NaOH, AR) and hydrochloric acid (HCl, AR) were purchased from Sinopharm Chemical Reagent Co., Ltd. All chemicals were used as received without further purification. Deionized (DI) water used in all the studies was purified by a Milli-Q water purification system.

4.2 Design and fabrication of microfluidic chips

Microfluidic chips used for one-step biofunctionalized QD synthesis were fabricated through soft-lithography and replica-molding methods[4, 10]. Briefly, negative photoresist SU-8 (GM1070, Gersteltec Engineering Solutions, Swiss) was spin coated onto a 4-inch silicon wafer (Semiconductor Wafer, Inc. Taiwan), followed by UV patterning of the channels (3min, lamp power: 355W) to form a master. The wafer was then developed using the AZ developer (Branchburg, NJ) to remove the unexposed photoresist. PDMS mixture containing curing agent and base resin (Dow Corning, US) with a weight ratio of 1:10 was poured onto the master and cured at 120℃ for 10 mins. The cured PDMS layer with microfluidic channels was then carefully peeled off from the master and stamped onto a glass slide.

4.3 Bench-top synthesis of MPA-CdTe QDs, BSA-CdTe QDs and FA-CdTe QDs

Te precursor was prepared by reducing 4 mg of tellurium powder with 10 mg of sodium borohydride ($NaBH_4$) in 1ml nitrogen-saturated DI water at room temperature. The mixture was stirred for 1-2 hours until it became colorless.

MPA-CdTe QDs were synthesized by our previous reported method in Ref [40, 50]. Briefly, 31mg of cadmium perchlorate, 17μL of MPA with concentrations ranging from 0 mM to 0.2 mM and 20 ml of nitrogen-saturated water were loaded into a three-necked flask under

stirring. The pH was adjusted to 9 by adding dropwise sodium hydroxide solution. The flask was sealed and subsequently the Te precursor was injected into the mixture under nitrogen atmosphere. The reaction mixture was slowly heated under nitrogen atmosphere to 98 ℃. After 2 mins, 10 mL of mixture solution was collected as MPA-CdTe QDs nucleates for later microfluidic synthesis. We have measured the UV-Vis and PL spectrum of MPA-CdTe QD nucleates. These spectra revealed a very weak feature of QDs. Such nucleates are very unstable and easy to be precipitated out from the water as time progresses.

To synthesize BSA-CdTe QDs, BSA stock solution (100 mg/mL) was first prepared by dissolving protein powder (BSA) in 1×PBS. For QD synthesis, 2 mL of BSA (concentration: 0, 0.25, 0.5, 1.0, 2.0 or 5.0 mg/mL) was added together with 31 mg of Cadmium perchlorate, 17μL of MPA with concentrations ranging from 0 mM to 0.2mM and 20 ml of nitrogen-saturated water into a three-necked flask under stirring at room temperature. The pH value of the mixture was adjusted to 9 by dropwise titration with sodium hydroxide solution. After quick injection of fresh Te precursor, the reaction mixture was vigorously stirred and heated to 65 ℃ under nitrogen atmosphere. Within 2 mins, 10 mL of mixture solution was collected as BSA-QD nucleates for later microfluidic synthesis. We have measured the UV-Vis and PL spectrum of BSA-CdTe QD nucleates. These spectra revealed a very weak feature of QDs. Such nucleates are very unstable and easy to be precipitated out from the water as time progresses. The synthesis protocol of folic acid (FA)-functionalized CdTe is same as BSA-CdTe QDs except that BSA stock solution was replaced by folic acid stock solution with concentrations of 0, 0.8, 1.6, 3.2, 6.4 mg/mL.

4.4 Microfluidic synthesis of MPA-CdTe QDs, BSA-CdTe QDs and FA-CdTe QDs

Solutions containing MPA-CdTe QDs, BSA-CdTe QDs and FA-CdTe QDs nucleates were firstly obtained as described in section 4.3. A syringe pump was used to inject nucleate reagents into the inlet of the microfluidic chips with a constant flow rate of 500 μL/min . The MPA-CdTe QDs, BSA-CdTe QDs and FA-CdTe QDs were respectively formed as the reaction mixture flowed continuously through the microfluidic channel which was heated from below using a hot plate with different temperatures of 98 ℃, 150 ℃, 180 ℃, 200 ℃, 220 ℃ for different batches of MPA-CdTe QDs and 50 ℃, 65 ℃, 85 ℃, 100 ℃ for different batches of BSA-CdTe QDs and FA-CdTe QDs. During the optimization process for the channel width of the microfluidic chips (200 μm, 400 μm, 600 μm) in QDs syntheses, we fixed the channel length at 800 mm and the reaction temperature at an optimum value of

180 ℃ for MPA-CdTe QDs and 65 ℃ for BSA-CdTe QDs and FA-CdTe QDs.

4.5 Purification of QDs

QD samples were mixed with equal amount of ethanol and then centrifuged at 10000 rpm for 5min to remove unreacted precursors and free ligand molecules. A centrifugal device with 100 kDa cut-off filter was used for purifying BSA-CdTe QDs. 3kDa cut-off filters were used to purify MPA-CdTe QDs and FA-CdTe QDs.

4.6 Optical characterization

The photoluminescence emission spectra of QDs were measured by a Fluorolog-3 Fluorometer (HORIBA Jobin Yvon, Edison, NJ USA) with an excitation wavelength of 400 nm. UV-Visible absorption spectra were collected using a spectrophotometer (Shimadzu UV-2450). Fourier transform infrared (FT-IR) spectra were obtained from a Shimadzu FT-IR spectrometer. In the FT-IR characterization, the QDs powder was mixed with potassium bromide (KBr) at 1:10 (w/w), grinded and compressed into tablets.

4.7 Simulation of QDs reaction in the microfluidic chips

To assess the performance of our designed microfluidic chips for QDs reaction, we simulated the laminar flow inside the MF channel using finite element method (FEM) software (COMSOL Multiphysics 4.3a). The simulation studies were carried out by coupling the Navier–Stokes equation (Eq. (3)), the continuity equation (Eq. (4)) and the mass balance equation (Eq. (5)).

$$-\nabla\cdot\mu\left(\nabla u+\left(\nabla u\right)^{T}\right)+\rho\left(u\cdot\nabla\right)u+\nabla p=F \tag{3}$$

$$\nabla\cdot u=0 \tag{4}$$

$$\nabla\cdot\left(-D\nabla c+cu\right)=0 \tag{5}$$

In the above equations, μ is the viscosity, u the velocity, ρ the density, p the pressure, F the sum of the body forces, D the diffusion coefficient, and c the concentration. These equations were solved for the 3D geometry as shown in Fig. 2. The diffusion coefficient (D) was set to $5\times10^{-7}e^{(-2000/T)}$. T is the temperature of reaction (K). The fluid density (ρ) and fluid viscosity (μ) were set as the default values of water that are related to T. For the Navier–Stokes

equation, a flow rate of 500 μL/min at the inlet was used. According to the boundary conditions, the velocity was zero at the channel walls. To solve the mass balance equation, a concentration of 10 mM of Cd^{2+} reactive species and 3.3 mM of Te^{2-} reactive species at the inlet were used.

4.8 Calculation of QDs particle number per liter

We first calculated the molar concentration of CdTe nanocrystals using the Lambert-Beer's law.

$$C = \frac{A}{\varepsilon L} \tag{6}$$

In Eq. (6), *C* is the molar concentration of the CdTe nanocrystals. *A* is the absorbance at the absorption peak of our CdTe sample solution. *L* is the path length of the radiation beam and here was fixed at 1 cm. ε is the extinction coefficient per mole of nanocrystals. In our calculation, the ε value is based on Eq. (7), an empirical function of the size of the CdTe nanocrystals from Peng et al. [49]. Here, we assumed the particle size was 1.5 nm.

$$\varepsilon = 10043(D)^{2.12} \tag{7}$$

Then, we use Eq. (8) to obtain the particle number of CdTe QDs per liter.

$$n_p = \frac{N}{V} = \frac{n}{V}N_A = \frac{CV}{V}N_A = CN_A \tag{8}$$

In Eq. (8), n_p is the particle number of the CdTe nanocrystals per liter. *V* is the volume of the CdTe sample solution. *N* is the particle number of the CdTe nanocrystals. N_A is the Avogadro constant. *n* is the amount of CdTe nanocrystals. *C* is the molar concentration of the CdTe nanocrystals.

4.9 Photostability and colloidal stability measurements of QDs

For the photostability measurements, QDs samples were continuously excited by a G10T8 UV lamp (Watts: 10W, Spectral Output: 254nm) and the photoluminescence emission spectra were recorded once every hour. For the colloidal stability measurements, the QDs after purification were dispersed in solutions with different pH values (5, 7, 9, and 12). A 90Plus particle size analyzer (Brookhaven Instruments, NY USA) was used in this study. The photoluminescence emission spectra and DLS data were recorded once every 12 hours.

4.10 Agarose gel electrophoresis

The QD sample used for agarose gel electrophoresis was mixture of 10 μL of purified QD solution with 30 μL of sodium hydroxide solution (pH=12). The running buffer was obtained by mixing 1% agarose gel with 1×TAE solution (Tris-Acetate-EDTA). The QD sample was then loaded into the running buffer and electrophoresed at a constant voltage of 110 V for 15 min at room temperature.

4.11 Cellular uptake of MF-BSA-QDs and MF-FA-QDs study

RAW264.7 macrophage cells and human pancreatic cancer cells, Panc-1 (CRL-1469, American Type Culture Collection) were cultured with Dulbecco's Modified Eagle's Medium (DMEM, Hyclone), supplemented with 10% fetal bovine serum (FBS, Hyclone), penicillin (100 μg ml^{-1}, Gibco) and streptomycin (100 μg ml^{-1}, Gibco) in a humidified environment (37 ℃, 5% CO_2). Before treating with QDs, cells were seeded onto cover glasses in a 6-well plate with DMEM medium. The prepared QD formulations were then diluted with PBS buffer (pH=7.2) solution to a concentration range of 10 to 20μg/mL. Next, the cells were treated with the QD formulations for 4h. After 4h of incubation, the treated cells were washed with PBS buffer for three times. Nikon Eclipse Ti inverted Microscope with 40x and 20x oil-immersion lens was used for macrophage and Panc-1 cell imaging study. The cytotoxicity of MF-BSA-QD formulations was also evaluated by MTT assays (Figure S3).

Reference

1. G. M. Whitesides, *Nature*, 2006, **442**, 368-373.
2. A. J. deMello, *Nature*, 2006, **442**, 394-402.
3. K. S. Elvira, X. C. i. Solvas, R. C. R. Wootton and A. J. deMello, *Nature Chemistry*, 2013, **5**, 905-915.
4. P. Song, D. Jian, H. Tng, R. Hu, G. Lin, E. Meng and K.-T. Yong, *Advanced Healthcare Materials*, 2013, **2**, 1170-1178.
5. J. Yan, M. Hu, D. Li, Y. He, R. Zhao, X. Jiang, S. Song, L. Wang and C. Fan, *Nano Res.*, 2008, **1**, 490-496.
6. A. D. Stroock, S. K. W. Dertinger, A. Ajdari, I. Mezić, H. A. Stone and G. M. Whitesides, *Science*, 2002, **295**, 647-651.
7. K. S. Krishna, Y. Li, S. Li and C. S. S. R. Kumar, *Advanced Drug Delivery Reviews*, 2013, **65**, 1470-1495.
8. S. Yao, Y. Shu, Y.-J. Yang, X. Yu, D.-W. Pang and Z.-L. Zhang, *Chemical Communications*, 2013, **49**, 7114-7116.

9. V. Vickerman, J. Blundo, S. Chung and R. Kamm, *Lab on a Chip*, 2008, **8**, 1468-1477.
10. T. Danny Jian Hang, P. Song, R. Hu, C. Yang and K.-T. Yong, *Analyst*, 2014, **139**, 407-415.
11. D. J. H. Tng, R. Hu, P. Song, I. Roy and K.-T. Yong, *Micromachines*, 2012, **3**, 615-631.
12. P. Song, R. Hu, D. J. H. Tng and K.-T. Yong, *RSC Advances*, 2014, **4**, 11499-11511.
13. J. B. Edel, R. Fortt, J. C. deMello and A. J. deMello, *Chemical Communications*, 2002, 1136-1137.
14. J. Huang, L. Lin, Q. Li, D. Sun, Y. Wang, Y. Lu, N. He, K. Yang, X. Yang, H. Wang, W. Wang and W. Lin, *Industrial & Engineering Chemistry Research*, 2008, **47**, 6081-6090.
15. X. Z. Lin, A. D. Terepka and H. Yang, *Nano Letters*, 2004, **4**, 2227-2232.
16. S. E. Lohse, J. R. Eller, S. T. Sivapalan, M. R. Plews and C. J. Murphy, *ACS Nano*, 2013, **7**, 4135-4150.
17. J. Wagner and J. M. Kohler, *Nano Letters*, 2005, **5**, 685-691.
18. Y. Song, L. L. Henry and W. Yang, *Langmuir*, 2009, **25**, 10209-10217.
19. Y. Song, H. Modrow, L. L. Henry, C. K. Saw, E. E. Doomes, V. Palshin, J. Hormes and C. S. S. R. Kumar, *Chemistry of Materials*, 2006, **18**, 2817-2827.
20. T. H. Eun, S.-H. Kim, W.-J. Jeong, S.-J. Jeon, S.-H. Kim and S.-M. Yang, *Chemistry of Materials*, 2009, **21**, 201-203.
21. M. Takagi, T. Maki, M. Miyahara and K. Mae, *Chemical Engineering Journal*, 2004, **101**, 269-276.
22. H. Wang, H. Nakamura, M. Uehara, M. Miyazaki and H. Maeda, *Chemical Communications*, 2002, 1462-1463.
23. L. Frenz, A. El Harrak, M. Pauly, S. Bégin-Colin, A. D. Griffiths and J.-C. Baret, *Angewandte Chemie International Edition*, 2008, **47**, 6817-6820.
24. S. A. Khan, A. Günther, M. A. Schmidt and K. F. Jensen, *Langmuir*, 2004, **20**, 8604-8611.
25. E. M. Chan, A. P. Alivisatos and R. A. Mathies, *Journal of the American Chemical Society*, 2005, **127**, 13854-13861.
26. E. M. Chan, R. A. Mathies and A. P. Alivisatos, *Nano Letters*, 2003, **3**, 199-201.
27. M. Mirhosseini Moghaddam, M. Baghbanzadeh, A. Sadeghpour, O. Glatter and C. O. Kappe, *Chemistry – A European Journal*, 2013, **19**, 11629-11636.
28. B. H. Kwon, H. Kim, Y. Kim, D. Kang and D. Young Jeon, *ECS Solid State Letters*, 2013, **2**, R27-R30.
29. A. M. Nightingale and J. C. de Mello, 2009, **10**, 2612-2614.
30. H. Wang, X. Li, M. Uehara, Y. Yamaguchi, H. Nakamura, M. Miyazaki, H. Shimizu and H. Maeda, *Chemical Communications*, 2004, 48-49.
31. A. Abou-Hassan, R. Bazzi and V. Cabuil, *Angew. Chem. Intl. Ed*, 2009, **48**, 7180-7183.
32. B.-H. Kwon, K. G. Lee, T. J. Park, H. Kim, T. J. Lee, S. J. Lee and D. Y. Jeon, *Small*, 2012, **8**, 3257-3262.
33. M. Uehara, H. Nakamura and H. Maeda, in *World Congress on Medical Physics and Biomedical Engineering 2006*, eds. R. Magjarevic and J. H. Nagel, Springer Berlin Heidelberg, 2007, 14, 250-253.
34. A. M. Nightingale and J. C. de Mello, *Journal of Materials Chemistry*, 2010, **20**, 8454-8463.

35. P. M. Valencia, O. C. Farokhzad, R. Karnik and R. Langer, *Nature Nanotechnology*, 2012, **7**, 623-629.
36. X. G. Peng, *Nano Res.*, 2009, **2**, 425-447.
37. P. N.Prasad, *Nanophotonics*, Hoboken : John Wiley & Sons, 2004.
38. P. N.Prasad, *Introduction to nanomedicine and nanobioengineering*, Hoboken, N.J. : Wiley, 2013.
39. X. Wang, W. W. Yu, J. Zhang, J. Aldana, X. Peng and M. Xiao, *Physical Review B*, 2003, **68**, 125318.
40. Y. Wang, R. Hu, G. Lin, W.-C. Law and K.-T. Yong, *RSC Advances*, 2013, **3**, 8899-8908.
41. S. Rauf, A. Glidle and J. M. Cooper, *Chemical Communications*, 2010, **46**, 2814-2816.
42. J. K. Jaiswal and S. M. Simon, *Trends in Cell Biology*, 2004, **14**, 497-504.
43. C. X. Guo, H. B. Yang, Z. M. Sheng, Z. S. Lu, Q. L. Song and C. M. Li, *Angewandte Chemie-International Edition*, 2010, **49**, 3014-3017.
44. C. X. Guo, J. Xie, B. Wang, X. Zheng, H. B. Yang and C. M. Li, *Scientific Reports*, 2013, **3**, 2957.
45. C. X. Guo, D. Zhao, Q. Zhao, P. Wang and X. Lu, *Chemical Communications*, 2014, DOI: 10.1039/C4CC01603C.
46. S. Zeng, D. Baillargeat, H.-P. Ho and K.-T. Yong, *Chemical Society Reviews*, 2014, **43**, 3426-3452.
47. T. Zhao, X. Hou, Y.-N. Xie, L. Wu and P. Wu, *Analyst*, 2013, **138**, 6589-6594.
48. Y. Nakane, A. Sasaki, M. Kinjo and T. Jin, *Analytical Methods*, 2012, **4**, 1903-1905.
49. W. W. Yu, L. H. Qu, W. Z. Guo and X. G. Peng, *Chemistry of Materials*, 2003, **15**, 2854-2860.
50. W.-C. Law, K.-T. Yong, I. Roy, H. Ding, R. Hu, W. Zhao and P. N. Prasad, *Small*, 2009, **5**, 1302-1310.
51. B. J. Kirby, *Micro- and Nanoscale Fluid Mechanics: Transport in Microfluidic Devices*, Cambridge University Press, New York, 2010.
52. A. Barth, *Biochimica et Biophysica Acta (BBA) - Bioenergetics*, 2007, **1767**, 1073-1101.
53. S. Hinds, B. J. Taft, L. Levina, V. Sukhovatkin, C. J. Dooley, M. D. Roy, D. D. MacNeil, E. H. Sargent and S. O. Kelley, *Journal of the American Chemical Society*, 2006, **128**, 64-65.
54. B. A. Kairdolf, A. M. Smith and S. Nie, *Journal of the American Chemical Society*, 2008, **130**, 12866-12867.
55. L. Ye, K. T. Yong, L. W. Liu, I. Roy, R. Hu, J. Zhu, H. X. Cai, W. C. Law, J. W. Liu, K. Wang, J. Liu, Y. Q. Liu, Y. Z. Hu, X. H. Zhang, M. T. Swihart and P. N. Prasad, *Nature Nanotechnology*, 2012, **7**, 453-458.
56. B. Zhang, R. Hu, Y. Wang, C. Yang, X. Liu and K.-T. Yong, *RSC Advances*, 2014, **4**, 13805-13816.